RSC Advances

PAPER

View Article Online
View Journal | View Issue

Cite this: *RSC Adv.*, 2024, **14**, 35628

Zeolitic imidazolate framework-67 in chitosan-grafted hydrogel as an effective catalyst for peroxymonosulfate activation to degrade antibiotics and dyes †

Atipong Nachaichot [a] Kunlarat Phonlakan [a] Supinya Nijpanich [b] Soraya Pornsuwan [c] and Surangkhana Budsombat *[a]

Zeolitic imidazolate framework-67 (ZIF-67) was synthesized *in situ* in the hydrogel of chitosan-grafted poly(acrylic acid) (chitosan-*g*-PAA) to activate peroxymonosulfate (PMS) and degrade tetracycline (TC). The catalytic performance of the composite hydrogel for TC degradation was evaluated under different conditions. The results showed rapid degradation, with enhanced degradation efficiency as the catalyst dosage, PMS dosage, and temperature increased. TC was degraded entirely within 30 min for catalyst and PMS dosages of 1 and 1 g per L, respectively. The composite hydrogel was effective across a broad pH range. A scavenging study and electron paramagnetic resonance experiments indicated that $SO_4^{\bullet-}$, $HO^{\bullet}$, $O_2^{\bullet-}$ and $^1O_2$ were involved in the degradation process. The antibacterial test against *E. coli* showed that the products of the TC degradation were nontoxic. Additionally, the composite hydrogel was evaluated in the presence of anions and in real water samples. The reusability study showed that the composite hydrogel could be recovered through filtration and effectively used for five consecutive cycles. Moreover, the composite hydrogel could degrade 82% ciprofloxacin and 86% norfloxacin, while it could completely degrade rhodamine B, reactive red 141, and methylene blue dyes within 30 min.

Received 10th September 2024
Accepted 3rd November 2024

DOI: 10.1039/d4ra06537a

rsc.li/rsc-advances

1. Introduction

High levels of antibiotics are discharged into water due to the growth of the pharmaceutical industry and animal husbandry. Tetracycline (TC), an antibiotic, is widely utilized to treat animal and human diseases and promote animal and plant growth.[1] However, TC is highly water-soluble, chemically stable, and non-biodegradable,[2] which is harmful to human health and the environment.[3] Several wastewater treatment processes, including adsorption, membrane technologies, and advanced oxidation processes (AOPs), can remove or degrade antibiotics.[4]

AOPs are potential approaches as they do not generate secondary toxic waste to be deposited into the environment. Hydroxyl radicals are produced in AOPs to degrade organic pollutants into nontoxic molecules, which can be mineralized into carbon dioxide and water. In recent years, sulfate radical-based advanced oxidation processes (SR-AOPs) have received much attention because they offer a strong oxidizing capacity and a broad working pH range with a long lifetime.[5,6] Sulfate radicals can be generated using various methods, including photolysis, pyrolysis, radiolysis, and activation of peroxymonosulfate (PMS).[7]

Although direct PMS activation is slow and requires energy,[8] combining PMS and transition metals, including Co, Mn, Ni, Fe, and Cu, is effective. Co demonstrated higher activation performance than other transition metals since the redox potential of Co was similar to that of PMS. Nevertheless, homogeneous Co catalysts have the potential toxicity of Co leaching and difficult metal recovery. Consequently, heterogeneous Co-based catalysts are being developed to overcome the limitations.[9,10] Zeolitic imidazolate framework-67 (ZIF-67) has been introduced as a PMS activator for degrading dyes and antibiotics. ZIF-67 is a porous metal–organic framework material composed of Co as the metal center and 2-methylimidazole (2-Mim) as the ligand.[11] The high porosity and abundance of Co ions make ZIF-67 an effective PMS activator in SR-AOPs.[12] However, separating ZIF-67 from wastewater is challenging. Therefore, this issue is addressed by combining ZIF-67 with $NiCo_2O_4$ nanocage,[13] Fe_2O_3 nanoparticles,[14] and Ti-based

[a]*Department of Chemistry and Center of Excellence for Innovation in Chemistry, Materials Chemistry Research Center, Faculty of Science, Khon Kaen University, Khon Kaen 40002, Thailand. E-mail: surama@kku.ac.th; Tel: +66-4300 9700. ext. 42174*

[b]*Synchrotron Light Research Institute (Public Organization), Nakhonratchasima 30000, Thailand*

[c]*Department of Chemistry and Center of Excellence for Innovation in Chemistry, Faculty of Science, Mahidol University, 272 Rama VI Rd., Ratchathewi, Bangkok 10400, Thailand*

† Electronic supplementary information (ESI) available. See DOI: https://doi.org/10.1039/d4ra06537a

membranes[15] to degrade TC, ciprofloxacin, and sulfamethoxazole, respectively.

This study synthesized ZIF-67 *in situ* in chitosan-grafted poly(acrylic acid) (chitosan-*g*-PAA) hydrogel. The obtained composite hydrogel was used to activate PMS in the TC degradation. Since chitosan-*g*-PAA hydrogel demonstrated a high mechanical strength, high water stability, and high adsorption capacity toward Co(II) ions, it was chosen to support ZIF-67.[16] This study first reported the *in situ* synthesis of ZIF-67 in a hydrogel for applications in SR-AOPs. The catalytic ability of the ZIF-67 composite hydrogel in the TC degradation was investigated. The influence of catalyst dosage, PMS dosage, initial TC concentration, pH, and temperature on the TC degradation was evaluated. The generation of reactive oxygen species was examined using scavenging and electron paramagnetic resonance (EPR) experiments. Furthermore, the catalytic system was tested in real water samples. Additionally, the impact of inorganic anions on TC degradation was discussed. The reusability of the composite catalyst was evaluated. Moreover, the catalytic performance of the composite toward other antibiotics was studied.

2. Experimental

2.1 Chemicals

Chitosan (≥75% deacetylation, 50 000–190 000 Da), PMS, acrylic acid (AA), and 2-Mim were obtained from Sigma-Aldrich. *N*,*N*′-methylenebis(acrylamide) (MBA) was purchased from Fluka. Loba Chemie supplied *t*-butanol and methylene blue. Potassium persulfate and cobalt(II) nitrate hexahydrate ($Co(NO_3)_2 \cdot 6H_2O$) were acquired from VWR and Guangdong Guanghua Chemical Factory, respectively. Ascorbic acid and sodium azide were purchased from Qrec. Sodium hydrogen carbonate and sodium nitrate were obtained from Ajax Finechem. Methanol and sodium chloride were obtained from RCI Labscan. TC, 5,5-dimethyl-1-pyrroline-*N*-oxide (DMPO), and 2,2,6,6-tetramethyl-4-piperidone (TEMP) were provided by TCI. Reactive red 141 was acquired from DyStar Singapore. Rhodamine B, ciprofloxacin, and norfloxacin were purchased from HiMedia, Millimed, and Masa Lab Co., Ltd, respectively.

2.2 Synthesis of ZIF-67 composite hydrogel

Chitosan-*g*-PAA hydrogel was synthesized, as mentioned in previous studies.[16] ZIF-67 was synthesized *in situ* in the hydrogel as follows: first, 2.1825 g (7.50 mmol) of $Co(NO_3)_2 \cdot 6H_2O$ was dissolved in deionized water (75 mL), followed by stirring the solution for 30 min. Then, the synthesized hydrogel was added to the solution and stirred for 4 h. In another beaker, 2.4600 g (29.96 mmol) of 2-Mim was dissolved in deionized water (25 mL), followed by slowly dropping this prepared 2-Mim solution into the hydrogel-containing solution. Afterward, the mixed solution was allowed to sit for 12 h. The obtained composite hydrogel was filtered, followed by thoroughly washing it with water and methanol to remove chemical residues and non-embedded ZIF-67 particles. Finally, the composite hydrogel was dried in an oven.

2.3 Procedures for degradation of TC

The TC degradation was performed using the ZIF-67 composite hydrogel as a catalyst. In a typical procedure, 1 g per L of the catalyst was added to 100 mL of a 10 mg per L TC solution for 30 min to establish adsorption–desorption equilibrium. The introduction of 0.3 g per L PMS solution initiated the TC degradation. The sample was collected and diluted with methanol, followed by subjecting it to ultraviolet-visible (UV-vis) measurements.

The influence of inorganic anions and water system on TC degradation was investigated under optimized conditions of 1 g per L catalyst dosage, 1 g per L PMS dosage, initial TC concentration of 10 mg per L, and 5 mM anion concentration to mimic the actual sewage solution.[17] Moreover, the catalytic ability of the composite was investigated in drinking water, tap water, and water from a facultative pond for wastewater treatment at Srinagarind Hospital, Khon Kaen. The composite was washed with water and methanol in the reusability test, followed by air-drying for the next experiment. The catalytic performance of the composite toward different antibiotics and dyes was studied using the initial pollutant concentration of 10 mg per L.

The degradation efficiency (in %) of the catalyst was determined from the concentration before degradation (C_0) and the concentration after degradation (C_t) using eqn (1).

$$\text{Degradation efficiency}(\%) = \frac{C_0 - C_t}{C_0} \times 100\% \quad (1)$$

2.4 Characterizations

Detailed information for Fourier transform infrared spectroscopy (FTIR), field emission scanning electron microscopy in conjunction with energy-dispersive X-ray spectroscopy (FESEM-

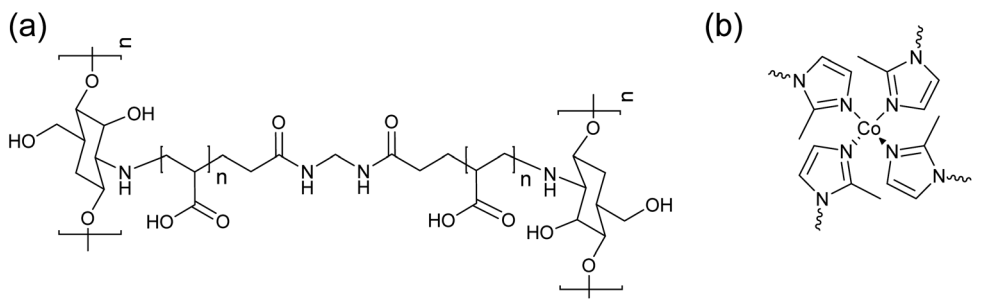

Fig. 1 Chemical structures of (a) the chitosan-*g*-PAA hydrogel and (b) ZIF-67.

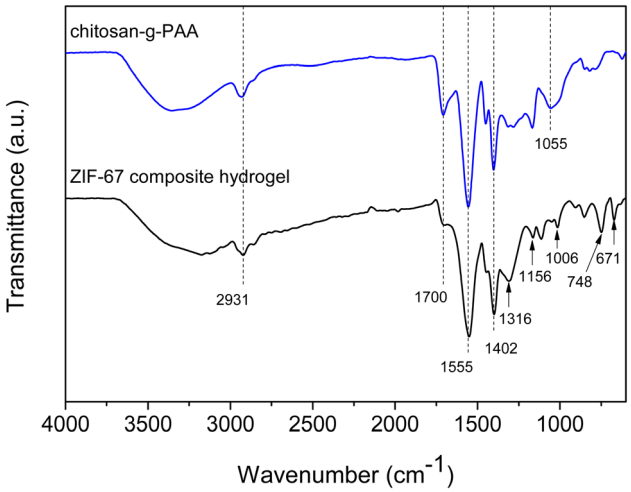

Fig. 2 FTIR spectra of chitosan-*g*-PAA and the ZIF-67 composite hydrogel.

EDS), thermogravimetric analysis (TGA), X-ray diffraction (XRD), X-ray photoelectron spectroscopy (XPS), atomic absorption spectrophotometry (AAS), UV-vis, and EPR has been presented in the ESI material (Text S1).† An antibacterial study was performed using the CLSI M2-A11 protocol against *Escherichia coli* (*E. coli*, strain ATCC 8739).

3. Results and discussions

3.1 Synthesis of the ZIF-67 composite hydrogel

The chitosan-*g*-PAA hydrogel was synthesized using the free radical graft copolymerization of AA with MBA as the cross-linking agent, according to the reported procedures.[16] The chemical structure of the hydrogel is depicted in Fig. 1(a) and FTIR confirmed its successful synthesis. As shown in the FTIR spectrum in Fig. 2, the amino and hydroxyl groups of chitosan were between 3000–3500 cm^{-1}, and its O–H bending was at 1055 cm^{-1}.[18] The band at 2931 cm^{-1} was attributed to the formation of the $-CH_2$ linkages in the copolymers and $-CH_2$ stretching of MBA.[18] The carbonyl stretching vibration appeared at 1700 cm^{-1}. The N–H deformation and the in-plane scissoring vibrations of CH_2 of MBA were at 1555 and 1402 cm^{-1}, respectively.[19] The chemical structure of ZIF-67 is shown in Fig. 1(b). The characteristic bands corresponding to ZIF-67 are shown in the FTIR spectrum of the ZIF-67 composite hydrogel in Fig. 2. The in-plane bending vibrations of the imidazole ring were at 1316,

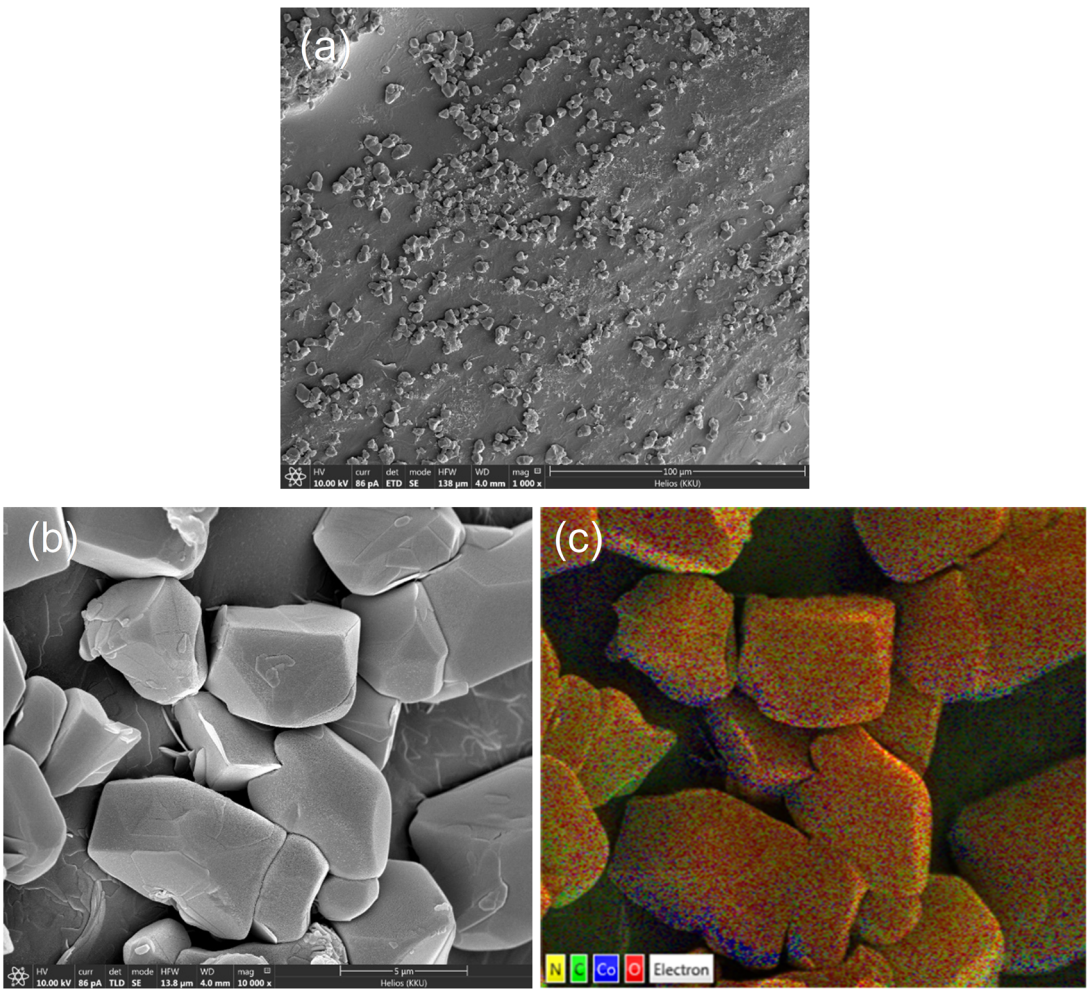

Fig. 3 SEM images of the ZIF-67 composite hydrogel at (a) 1000× and (b) 10 000× magnifications with elemental mapping (c).

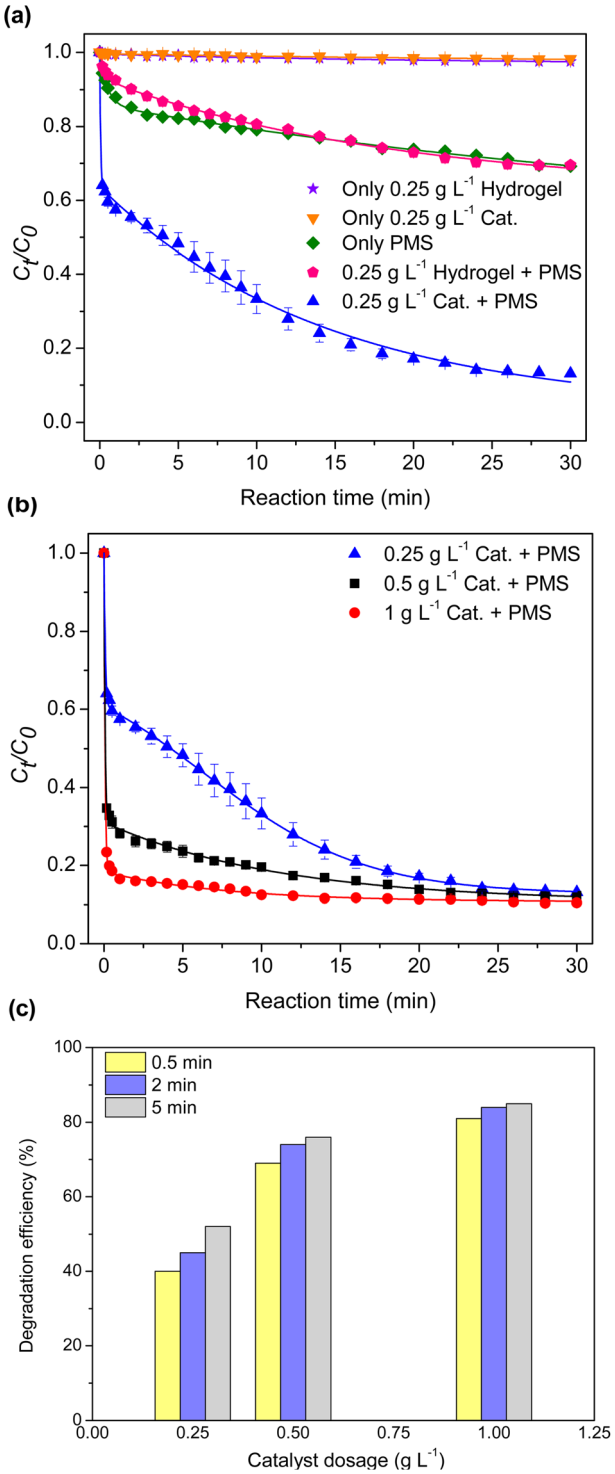

Fig. 4 Effects of degradation system (a) and catalyst dosage (b) with a correlation plot between time and degradation efficiency (c).

1156, and 1006 cm^{-1}.[20] The bands at 748 and 671 cm^{-1} were attributed to the out-of-plane bending of the imidazole ring.[21,22]

The morphology of ZIF-67 particles on the surface is illustrated in the SEM images of the composite hydrogel in Fig. 3(a and b). Elemental mapping in Fig. 3(c) revealed the presence of Co, C, and N, confirming the formation of ZIF-67. The average particle size was 3.7 μm, and particle aggregation was observed.

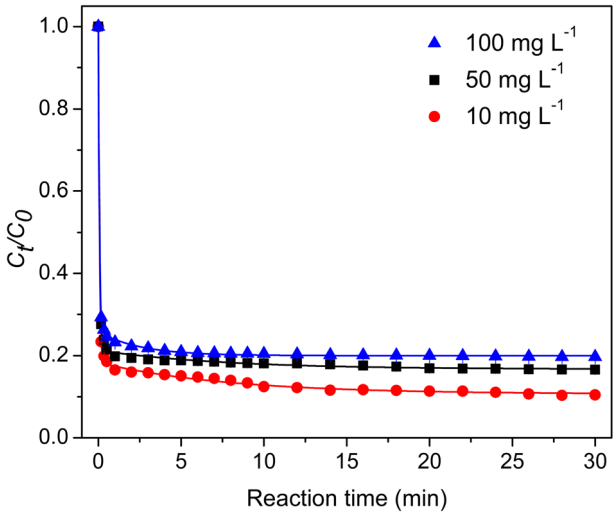

Fig. 5 Effect of the initial TC concentration.

The thermal stabilities of chitosan-*g*-PAA and the ZIF-67 composite hydrogel were analyzed using TGA and depicted in Fig. S1.† The bare hydrogel showed a multi-step decomposition, and the primary weight loss at 454 °C was attributed to the PAA decomposition.[16] The composite hydrogel showed two additional weight loss steps at 319 and 603 °C, which could be related to the escape of 2-Mim from the ZIF-67 surface,[23] and the major ZIF-67 decomposition,[24] respectively. The ZIF-67 content of 17.5% was determined from the difference between the residual weights of the bare hydrogel and the ZIF-67 composite hydrogel at 800 °C. The crystallinity of both the bare hydrogel and the composite hydrogel was analyzed using XRD. As shown in Fig. S2,† the XRD pattern of the bare hydrogel displayed a small broad peak in the range of 15–40°, which was attributed to a random crosslinking network.[25] Upon the *in situ* synthesis of ZIF-67 in the hydrogel, no noticeable peaks of ZIF-67 particles were observed. This could be due to the relatively low ZIF-67 content in the hydrogel.

3.2 TC degradation

3.2.1 Effect of catalyst dosage. The catalytic performance of the composite hydrogel was evaluated towards TC at a dosage of 0.25 g per L and compared with control experiments. As depicted in Fig. 4(a), only 2% of TC was removed when either the bare hydrogel or the composite catalyst was present, possibly due to the adsorption of TC. Additionally, 31% of TC was degraded after 30 min of reaction when only PMS was present due to the oxidizing properties of PMS. A similar extent of degradation was observed in the system containing PMS and bare hydrogel. This observation suggested that the bare hydrogel did not play a significant role in the degradation process of TC. Combining PMS and the composite catalyst resulted in a higher degradation rate and 87% degradation efficiency, revealing that the composite catalyst facilitated the PMS activation.

Furthermore, the impact of catalyst dosage on TC degradation was evaluated, and a correlation between time and

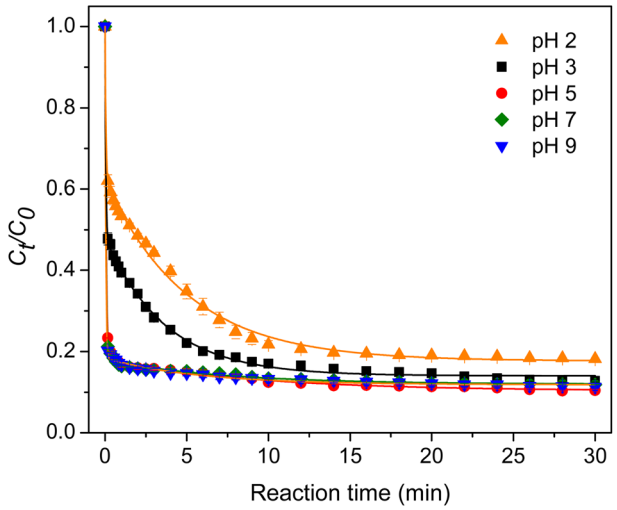

Fig. 6 Effect of pH.

degradation efficiency at the beginning of the degradation process was depicted in Fig. 4(b and c). The increased degradation rate as a function of the catalyst dosage was due to the increased active sites provided to PMS. At 1 g per L catalyst dosage, 81% of TC was rapidly degraded within 0.5 min, and the degradation efficiency reached 89% after 30 min.

3.2.2 Effect of the initial TC concentration. The influence of the initial TC concentration on its degradation was evaluated. As shown in Fig. 5, the degradation rate decreased as the initial concentration rose from 10 to 100 mg per L, and the degradation efficiency declined from 89% to 80%. The relatively constant quantity of reactive species generated from the same concentrations of catalyst and PMS in the reaction could explain this observation.[1] Notably, the high degradation rates and efficiencies were maintained despite the ten-fold increase in the initial TC concentration.

3.2.3 Effect of pH. The degradation ability of the composite hydrogel was evaluated in the pH range of 2–9. As displayed in Fig. 6, the TC degradation rate increased with the pH value up to pH 5.[17] The hydrogel surface was positively charged at a pH below 4.3 since the point of zero charge of chitosan-*g*-PAA was 4.3.[16] Under strong acidic conditions, the reaction between protons and PMS generated SO_2–O–O–H_2^+.[26] Therefore, the slow degradation was due to the repulsion between the two positively charged species. Furthermore, TC had three pK_a values, which were 3.3, 7.8, and 9.6.[27] TC was in the form of TCH_3^+ at a pH below 3.3. The electrostatic repulsion between the hydrogel and TC could account for the low degradation rate. The one-way analysis of variance (ANOVA) indicated that the degradation rate did not change significantly as the pH of the solution was further increased from 5 to 7 and 9 ($p < 0.05$). Therefore, the suitable pH of the solution for the composite hydrogel was in the 5–9 range.

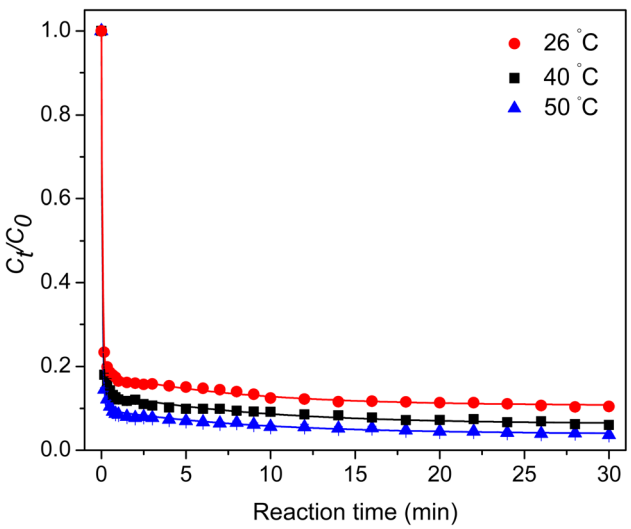

Fig. 7 Effect of temperature.

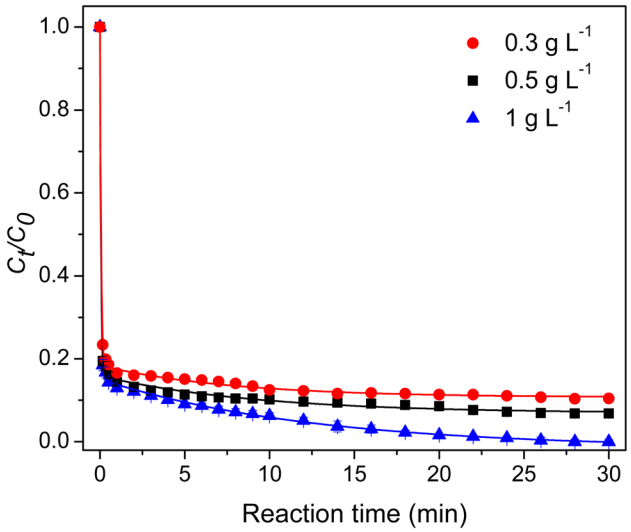

Fig. 8 Effect of the PMS dosage.

3.2.4 Effect of temperature. The effect of temperature on TC degradation was studied and is illustrated in Fig. 7. The TC degradation rate increased with the increase in temperature due to the increased collision frequency between the catalyst and TC. Additionally, this observation confirmed that the PMS activation was endothermic.

3.2.5 Effect of PMS dosage. The effect of PMS dosage on TC degradation was investigated using three different concentrations of PMS (0.3, 0.5, and 1 g per L). As shown in Fig. 8, the TC degradation rate increased with the increased PMS dosage. The increment was because the catalytic system generated an increased reactive oxygen species. A rapid TC degradation was observed within 1 min for the three PMS dosages. At 1 g per L PMS dosage, a complete TC degradation was achieved within 30 min. Table 1 reports the efficiencies of different Co-based PMS activators for TC degradation. The composite hydrogel showed similar performance compared to the other catalysts.

3.2.6 Effect of radical scavenger. Scavenging experiments employing methanol, *t*-butanol, ascorbic acid, and sodium azide as scavengers were conducted to understand the degradation process. Reportedly, methanol could quench $SO_4^{\bullet-}$ and HO$^\bullet$, while *t*-butanol selectively quenched HO$^\bullet$.[32,33] Ascorbic acid and sodium azide were used to quench superoxide radicals ($O_2^{\bullet-}$) and

Table 1 Comparison of different Co-based catalysts for TC degradation

Catalyst	$[TC]_0$ (mg L^{-1})	[Catalyst] (g L^{-1})	[PMS]	Performance	Ref.
Co/SiO_2	10	0.03	0.48 mM	46%, 20 min	28
Co@NC-800	30	0.2	0.2 g L^{-1}	90.1%, 3 min	29
Co@NCNTs-600	20	0.12	2 mM	93.1%, 20 min	30
ZCCN-30%	10	0.2	1 mM	99%, 40 min	31
BCFB@PCo/CoO	30	0.2	0.4 g L^{-1}	99.94%, 15 min	1
ZIF-67 in $NiCo_2O_4$ nanocage	20	0.05	0.3 g L^{-1}	99.58%, 30 min	13
ZIF-67 composite hydrogel	10	1	1 g L^{-1}	100%, 30 min	This study

singlet oxygen ($^1O_2$), respectively.[34] As depicted in Fig. 9(a), methanol, *t*-butanol, ascorbic acid, and sodium azide had an inhibiting effect, indicating that $SO_4^{\bullet-}$, $HO^{\bullet}$, $O_2^{\bullet-}$, and $^1O_2$ were generated in the catalytic degradation of TC. DMPO and TEMP were used as spin-trapping agents in EPR experiments. The presence of $SO_4^{\bullet-}$ and $HO^{\bullet}$ was evidenced from the seven-line spectrum characteristic of DMPOX (5,5-dimethyl-2-pyrrolidone-*N*-oxyl) (Fig. 9(b)).[35] The signals of DMPO-$O_2^{\bullet-}$ adduct were observed when DMPO and methanol were used.[36] Moreover, the generation of $^1O_2$ was confirmed by the triplet signal of TEMP-$^1O_2$.[37]

Furthermore, the ZIF-67 composite hydrogel was analyzed using XPS. The presence of the C 1s, N 1s, O 1s, and Co 2p peaks is indicated in the survey spectrum in Fig. 10(a). Chitosan and PAA in the hydrogel introduced the O 1s peak at 532.3 eV.[16] The N 1s peak at 399.1 eV was primarily due to ZIF-67.[38] The C 1s peak at 285.7 eV was due to the hydrogel and ZIF-67. As shown in Fig. 10(b), the Co 2p spectrum consisted of two major Co $2p_{1/2}$ and Co $2p_{3/2}$ peaks at 797.3 and 781.2 eV, respectively.[39] The peaks at 798.3 and 783.3 eV were assigned to Co^{2+}, while the peaks at 796.1 and 781.0 eV could be attributed to Co^{3+}.[40] Both Co^{2+} and Co^{3+} states can exist in ZIF-67 due to the adsorption/desorption with external molecules in water.[41] Moreover, shake-up satellite peaks were at 802.7 and 786.4 eV.[40]

The Co 2p spectrum of the used ZIF-67 composite hydrogel is shown in Fig. 10(c). The Co^{3+}/Co^{2+} ratio in the ZIF-67 composite hydrogel increased from 1.94 to 2.05, suggesting the participation of Co^{2+} and Co^{3+} in PMS activation. Co^{2+} reacted with PMS (HSO_5^-) to form Co^{3+} and $SO_4^{\bullet-}$. The generated Co^{3+} could be reduced to Co^{2+} to establish the Co^{2+}/Co^{3+} cycle. The possible degradation mechanisms activated using the ZIF-67 composite hydrogel and PMS are shown in eqn (2)–(11).[7,40,42]

$$Co^{2+} + HSO_5^- \rightarrow Co^{3+} + SO_4^{\bullet-} + OH^- \quad (2)$$

$$Co^{3+} + HSO_5^- \rightarrow Co^{2+} + SO_5^{\bullet-} + H^+ \quad (3)$$

$$SO_4^{\bullet-} + OH^- \rightarrow SO_4^{2-} + HO^{\bullet} \quad (4)$$

$$HSO_5^- + SO_5^{2-} \rightarrow HSO_4^- + SO_4^{2-} + {}^1O_2 \quad (5)$$

$$H_2O + HSO_5^- \rightarrow HSO_4^- + H_2O_2 \quad (6)$$

$$H_2O_2 \rightarrow H^+ + HO_2^{\bullet-} \quad (7)$$

$$HO_2^{\bullet-} \rightarrow H^+ + O_2^{\bullet-} \quad (8)$$

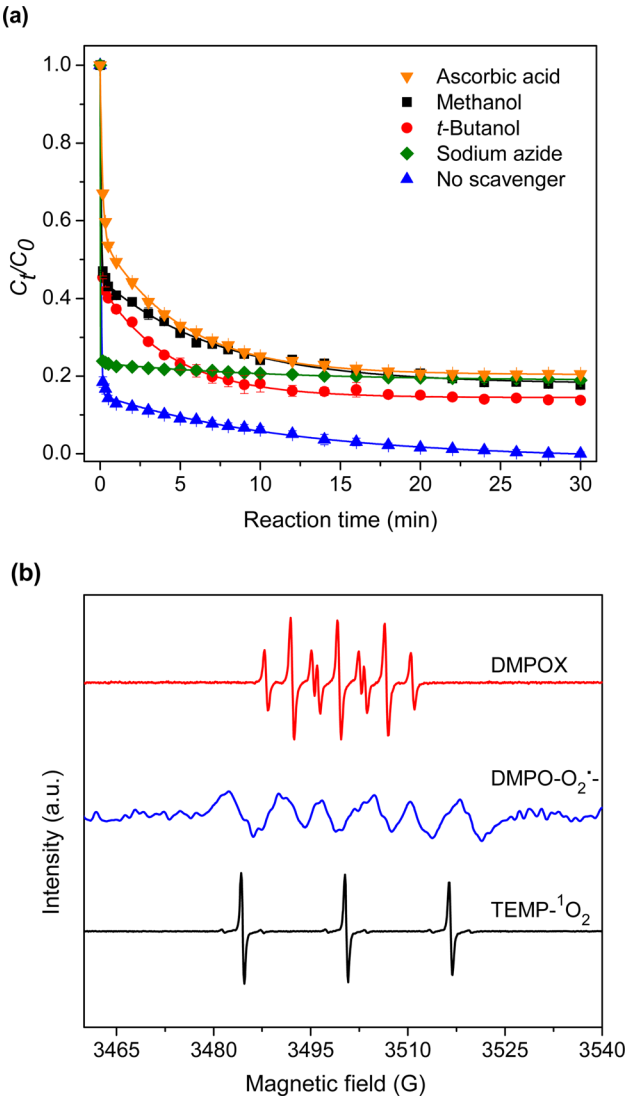

Fig. 9 (a) Effect of radical scavenger. [scavenger] = 20 mM, and (b) EPR spectra in ZIF-67 composite hydrogel/PMS systems.

$$2H^+ + 2O_2^{\bullet-} \rightarrow H_2O_2 + {}^1O_2 \quad (9)$$

$$HO^{\bullet} + O_2^{\bullet-} \rightarrow OH^- + {}^1O_2 \quad (10)$$

$$SO_4^{\bullet-} + HO^{\bullet} + O_2^{\bullet-} + {}^1O_2 + TC \rightarrow \text{intermediates} \rightarrow H_2O + CO_2 \quad (11)$$

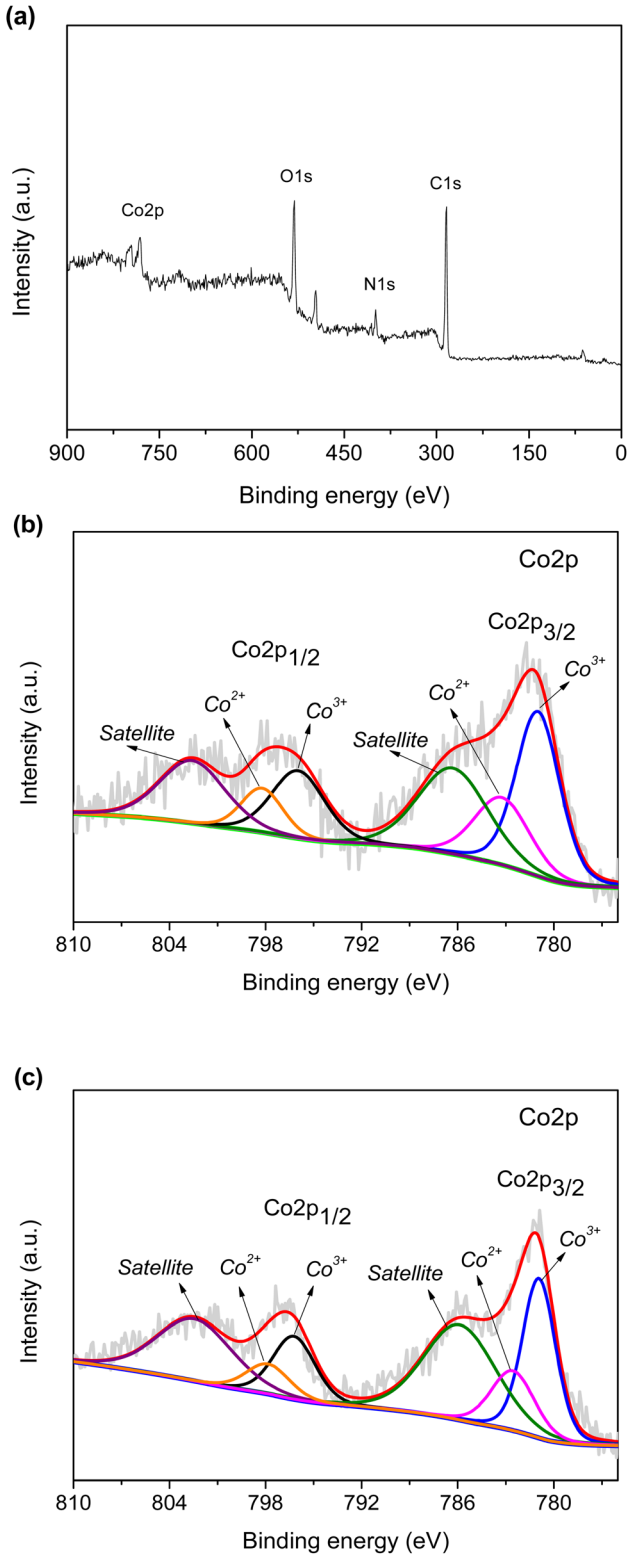

Fig. 10 (a) Survey XPS spectrum. Co 2p spectrum of (b) the fresh and (c) the used ZIF-67 composite hydrogel.

3.2.7 Effect of inorganic anions and the real water system evaluation. The impact of the commonly found anions in water on TC degradation was investigated. As depicted in Fig. 11(a), NO_3^- significantly affected the TC degradation rate. As shown in eqn (12)–(14), NO_3^- could react with $HO^\bullet$ or $SO_4^{\bullet-}$ to produce $NO_3^\bullet$ and $NO_2^\bullet$, decelerating the TC degradation.[43]

$$NO_3^- + HO^\bullet \rightarrow NO_3^\bullet + OH^- \quad (12)$$

$$NO_3^- + SO_4^{\bullet-} \rightarrow NO_3^\bullet + SO_4^{2-} \quad (13)$$

$$NO_3^\bullet + H_2O + e^- \rightarrow NO_2^\bullet + 2OH^- \quad (14)$$

The presence of Cl^-, SO_4^{2-}, or HCO_3^- decreased the TC degradation rate slightly. Cl^- could react with $SO_4^{\bullet-}$ to produce weaker chlorine oxidants (eqn (15)).[40,44]

$$Cl^- + SO_4^{\bullet-} \rightarrow SO_4^{2-} + Cl^\bullet \quad (15)$$

Although SO_4^{2-} could not react with sulfate radicals, it could reduce their reduction potential, leading to a slower

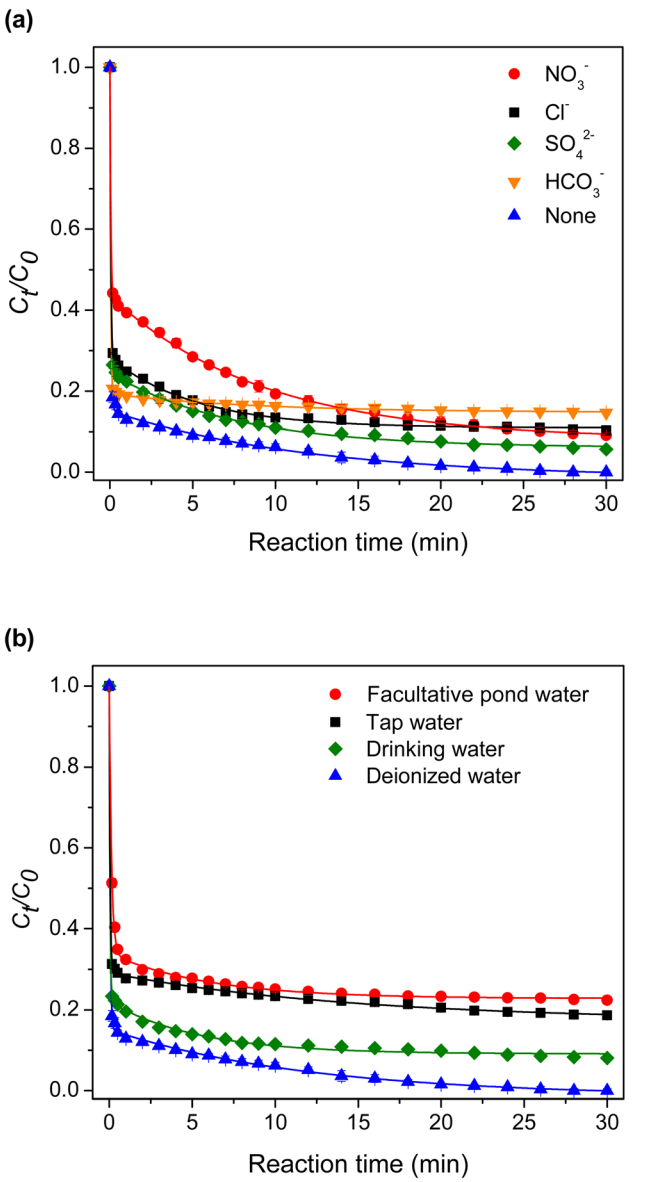

Fig. 11 Effects of (a) inorganic anions and (b) water systems.

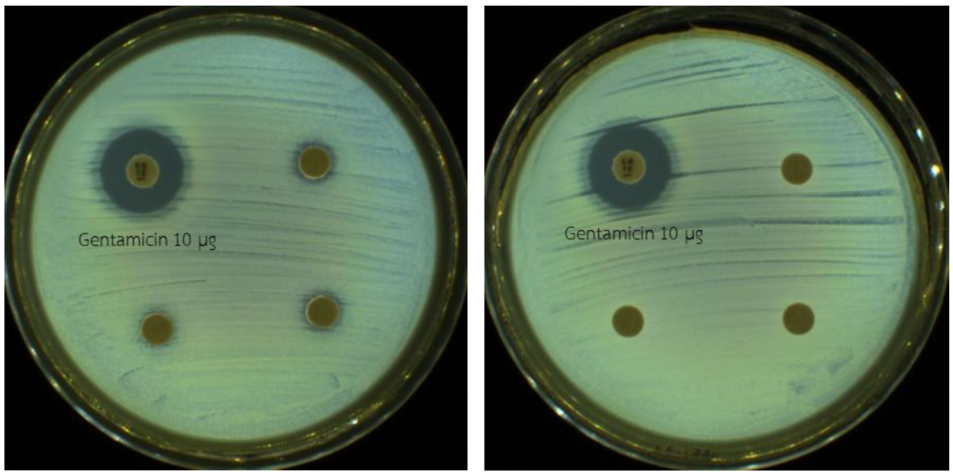

Fig. 12 Antibacterial activities against *E. coli* of the as-prepared TC solution (left) and residual TC solution after the degradation reaction that used the ZIF-67 composite hydrogel/PMS system (triplicate).

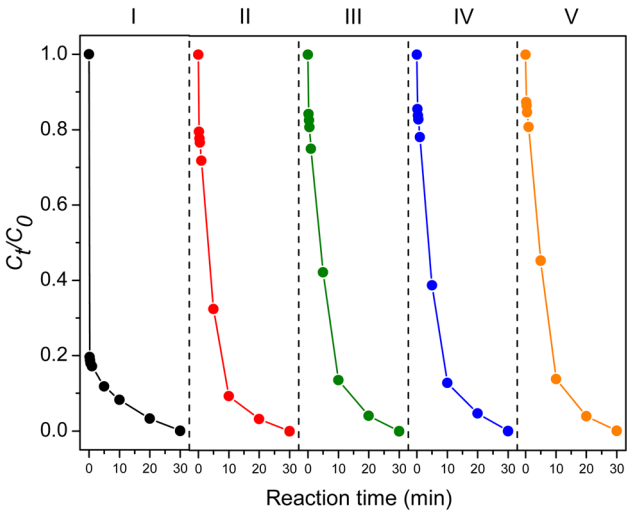

Fig. 13 Reusability of the ZIF-67 composite hydrogel.

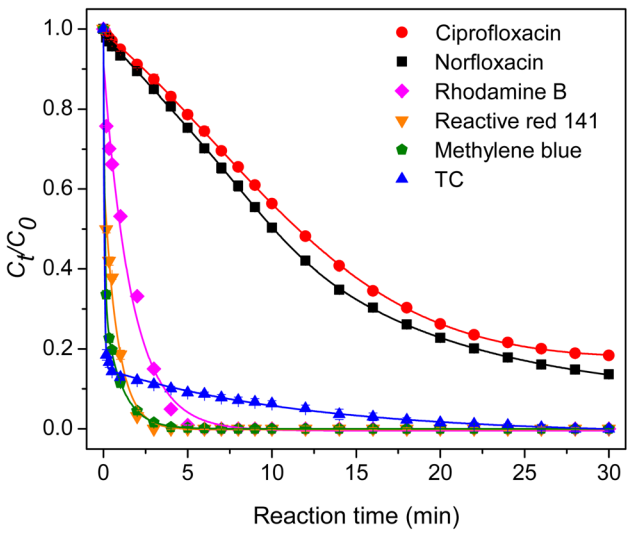

Fig. 14 Degradation of other antibiotics and dyes.

degradation.[45] As shown in eqn (16) and (17), HCO_3^- reacted with $HO^\bullet$ and $SO_4^{\bullet-}$ to generate the less active carbonate and bicarbonate radicals, respectively.[46]

$$HCO_3^- + HO^\bullet \rightarrow CO_3^{\bullet-} + H_2O \quad (16)$$

$$HCO_3^- + SO_4^{\bullet-} \rightarrow {}^\bullet HCO_3 + SO_4^{2-} \quad (17)$$

The catalytic ability was evaluated in the real water environment. As shown in Fig. 11(b), the effectiveness of the catalyst declined with the purity of water. The TC degradation rate decreased in the following order: deionized water > drinking water > tap water > facultative pond water. A high 78% degradation extent was achieved after 30 min of reaction for the test in facultative pond water.

3.2.8 Antibacterial test. The toxicity of the degradation products against *E. coli* was examined using an antibacterial test. The test compared the as-prepared TC solution (10 mg per L) and residual TC solution after a degradation reaction using the ZIF-67 composite hydrogel/PMS system, following the CLSI M2-A11 protocol. A positive control using 10 µg of Gentamicin was included. As shown in Fig. 12, no inhibition zones were produced by the degradation products, indicating nontoxicity.

3.2.9 Reusability. Furthermore, the reusability of the ZIF-67 composite hydrogel in PMS activation for TC degradation was studied. The composite hydrogel was washed with water and methanol, followed by air-drying for the next experiment. As shown in Fig. 13, the composite hydrogel could be used for five consecutive cycles with a slightly decreased degradation rate. The slower rate could be attributed to the loss of the catalyst during stirring and washing. The composite hydrogel remained intact, and the FTIR spectra showed no substantial change after five cycles (Fig. S3†). These observations indicated that the composite hydrogel was sufficiently stable under the studied degradation conditions. The cobalt leaching was analyzed using AAS. The Co^{2+} traces were 1.4 mg per L after the first cycle, and between 6.8 and 8.8 mg per L after cycles 2 to 5. Although these

values were comparable to those of other Co-based catalysts,[47] more efforts should be made to stabilize cobalt ions to meet the permissible limit for surface water.[48]

3.3 Degradation of other antibiotics and dyes

The catalytic performance of the ZIF-67 composite hydrogel toward different antibiotics and dyes was evaluated. As shown in Fig. 14, the composite hydrogel could degrade 82% ciprofloxacin and 86% norfloxacin within 30 min. Moreover, it could completely degrade rhodamine B, reactive red 141, and methylene blue dyes.

4. Conclusions

This study synthesized ZIF-67 *in situ* in chitosan-*g*-PAA hydrogel. FTIR and SEM confirmed the successful synthesis of ZIF-67, and the average particle size of ZIF-67 was 3.7 μm. TGA determined that the composite hydrogel had 17.5% ZIF-67 content. The ZIF-67 composite hydrogel could effectively activate PMS in the TC degradation. The degradation rate increased with the increased catalyst dosage, PMS dosage, and temperature. However, the TC concentration showed the opposite effect. TC was completely degraded for catalyst and PMS dosages of 1 and 1 g per L, respectively. Furthermore, the catalyst did not have significantly different degradation efficiencies when tested in the 5–9 pH range, suggesting its versatility. XPS analysis revealed the involvement of Co^{2+} and Co^{3+} in the degradation process. The scavenging study and EPR experiments indicated the production of $SO_4^{\bullet-}$, $HO^{\bullet}$, $O_2^{\bullet-}$, and $^1O_2$ in the catalytic system. When evaluated in real water samples and the presence of anions, the composite hydrogel maintained an above 78% degradation efficiency. The antibacterial test against *E. coli* indicated the nontoxicity of the products of the TC degradation. Moreover, the composite hydrogel could degrade other antibiotics and dyes. The composite hydrogel could be used for five cycles with a slightly decreased degradation rate.

Data availability

The manuscript includes all data supporting this article.

Conflicts of interest

There are no conflicts of interest to declare.

Acknowledgements

The authors gratefully acknowledge the financial support from the Materials Chemistry Research Center, Research and Graduate Studies, Khon Kaen University, and the Center of Excellence for Innovation in Chemistry (PERCH-CIC), Ministry of Higher Education, Science, Research and Innovation.

References

1 L. Dai, C. Cui, M. Yang, S. Jiang, J. Lan and R. Guo, *Water Sci. Technol.*, 2023, **88**, 2033–2053.
2 C. Xu, Q. Liu, M. Wei, S. Guo, Y. Fang, Z. Ni, X. Yang, S. Zhang and R. Qiu, *Sep. Purif. Technol.*, 2022, **295**, 121347.
3 H. Liu, Y. Yang, H. Sun, L. Zhao and Y. Liu, *Chemosphere*, 2018, **193**, 998–1003.
4 Y. Cong, X. Chen, L. Ye, X. Li and S.-W. Lv, *Chemosphere*, 2022, **307**, 136073.
5 R. Luo, M. Li, C. Wang, M. Zhang, M. A. Nasir Khan, X. Sun, J. Shen, W. Han, L. Wang and J. Li, *Water Res.*, 2019, **148**, 416–424.
6 W. Hu, Y. Xie, S. Lu, P. Li, T. Xie, Y. Zhang and Y. Wang, *Sci. Total Environ.*, 2019, **680**, 51–60.
7 J. Wang and S. Wang, *Chem. Eng. J.*, 2018, **334**, 1502–1517.
8 G. P. Anipsitakis and D. D. Dionysiou, *Environ. Sci. Technol.*, 2003, **37**, 4790–4797.
9 W. Zhao, Q. Shen, T. Nan, M. Zhou, Y. Xia, G. Hu, Q. Zheng, Y. Wu, T. Bian, T. Wei and C. Zhang, *J. Alloys Compd.*, 2023, **958**, 170370.
10 B. Li, Y.-F. Wang, L. Zhang and H.-Y. Xu, *Chemosphere*, 2022, **291**, 132954.
11 K. Y. Andrew Lin and B. C. Chen, *Dalton Trans.*, 2016, **45**, 3541–3551.
12 X. W. Zhang, M. Y. Lan, F. Wang, X. H. Yi and C. C. Wang, *J. Environ. Chem. Eng.*, 2022, **10**(3), 107997.
13 J. Pan, L. Che, T. Wei, Y. Cong and S.-W. Lv, *Appl. Surf. Sci.*, 2023, **637**, 157997.
14 B. Hashemzadeh, H. Alamgholiloo, N. Noroozi Pesyan, E. Asgari, A. Sheikhmohammadi, J. Yeganeh and H. Hashemzadeh, *Chemosphere*, 2021, **281**, 130970.
15 H. Ma, X. Li, Z. Pan, R. Xu, P. Wang, H. Li, Y. Shi, X. Fan and C. Song, *J. Membr. Sci.*, 2022, **661**, 120924.
16 P. Meetam, K. Phonlakan, S. Nijpanich and S. Budsombat, *Int. J. Biol. Macromol.*, 2024, **255**, 128261.
17 S. Bo, X. Zhao, Q. An, J. Luo, Z. Xiao and S. Zhai, *RSC Adv.*, 2019, **9**, 5009–5024.
18 Lalita, A. P. Singh and R. Kr. Sharma, *Int. J. Biol. Macromol.*, 2017, **105**, 1202–1212.
19 R. Blažic, D. Kučić Grgić, M. Kraljić Roković and E. Vidović, *Gels*, 2022, **8**, 636.
20 J. Cheng, D. Ma, S. Li, W. Qu and D. Wang, *Polymers*, 2020, **12**(2), 347.
21 C. Panawong, K. Phonlakan, S. Nijpanich, S. Pornsuwan and S. Budsombat, *J. Environ. Chem. Eng.*, 2023, **11**, 109909.
22 F. Verpoort, B. Mousavi, A. Zanon and S. Chaemchuen, *J. CO_2 Util.*, 2017, **20**, 282–291.
23 M. Davoodi, F. Davar, M. R. Rezayat, M. T. Jafari, M. Bazarganipour and A. E. Shalan, *RSC Adv.*, 2021, **11**, 13245–13255.
24 X. Qian, Q. Ren, X. Wu, J. Sun, H. Wu and J. Lei, *ChemistrySelect*, 2018, **3**, 657–661.
25 Y. Wang, J. Wang, Z. Yuan, H. Han, T. Li, L. Li and X. Guo, *Colloids Surf., B*, 2017, **152**, 252–259.
26 J. Deng, C. Ya, Y. Ge, Y. Cheng, Y. Chen, M. Xu and H. Wang, *RSC Adv.*, 2018, **8**, 2338–2349.
27 J. Chico, F. van Holthoon and T. Zuidema, *Chromatogr. Res. Int.*, 2012, **2012**, 1–9.

28 C. Panawong, A. Chatsri, A. Nachaichot, T. Nanmong, S. Loiha, S. Pornsuwan, S. Nijpanich, S. Mukdasai and S. Budsombat, *J. Mol. Liq.*, 2024, **407**, 125230.
29 J. Cao, Z. Yang, W. Xiong, Y. Zhou, Y. Wu, M. Jia, S. Sun, C. Zhou, Y. Zhang and R. Zhong, *Sep. Purif. Technol.*, 2020, **250**, 117237.
30 L. Hu, Y. Zhang, X. Liu, H. Zhu, J. Wu, Y. Wang, Y. Long and G. Fan, *Chem. Eng. J.*, 2022, **450**, 138219.
31 X. Li, S. Wang, B. Xu, X. Zhang, Y. Xu, P. Yu and Y. Sun, *Chem. Eng. J.*, 2022, **441**, 136074.
32 Z. Huang, H. Bao, Y. Yao, W. Lu and W. Chen, *Appl. Catal., B*, 2014, **154–155**, 36–43.
33 Y. Xue, N. N. T. Pham, G. Nam, J. Choi, Y. Y. Ahn, H. Lee, J. Jung, S. G. Lee and J. Lee, *Chem. Eng. J.*, 2021, **408**, 127305.
34 J. Su, L. Zhu, P. Geng and G. Chen, *J. Hazard. Mater.*, 2016, **316**, 159–168.
35 Q. Yang, P. Cui, C. Liu, G. Fang, M. Huang, Q. Wang, Y. Zhou, H. Hou and Y. Wang, *J. Hazard. Mater.*, 2021, **416**, 126215.
36 K. Tian, F. Shi, M. Cao, Q. Zheng and G. Zhang, *Catalysts*, 2022, **12**, 1058.
37 S. Afzal, K. Pan, D. Duan, Y. Wei and L. Chen, *Appl. Surf. Sci.*, 2021, **542**, 148674.
38 K. Phonlakan, S. Pornsuwan, S. Nijpanich and S. Budsombat, *Int. J. Biol. Macromol.*, 2024, **265**, 130922.
39 X.-D. Du, C.-C. Wang, J.-G. Liu, X.-D. Zhao, J. Zhong, Y.-X. Li, J. Li and P. Wang, *J. Colloid Interface Sci.*, 2017, **506**, 437–441.
40 J. Di, R. Jamakanga, Q. Chen, J. Li, X. Gai, Y. Li, R. Yang and Q. Ma, *Sci. Total Environ.*, 2021, **784**, 147258.
41 G. Saracco, S. Vankova, C. Pagliano, B. Bonelli and E. Garrone, *Phys. Chem. Chem. Phys.*, 2014, **16**, 6139–6145.
42 W. Ren, J. Gao, C. Lei, Y. Xie, Y. Cai, Q. Ni and J. Yao, *Chem. Eng. J.*, 2018, **349**, 766–774.
43 Q. Wang, Y. Shao, N. Gao, W. Chu, X. Shen, X. Lu, J. Chen and Y. Zhu, *Chem. Eng. J.*, 2016, **304**, 201–208.
44 L. Chen, X. Zuo, S. Yang, T. Cai and D. Ding, *Chem. Eng. J.*, 2019, **359**, 373–384.
45 J. Wang and S. Wang, *Chem. Eng. J.*, 2021, **411**, 128392.
46 G. Zhu, J. Zhu, X. Fu, Q. Liu, F. Cao, Y. Li, Q. Qin and M. Jiao, *Phys. Chem. Chem. Phys.*, 2020, **22**, 15340–15353.
47 N. T. Dung, T. V. Thu, T. Van Nguyen, B. M. Thuy, M. Hatsukano, K. Higashimine, S. Maenosono and Z. Zhong, *RSC Adv.*, 2020, **10**, 3775–3788.
48 L. Hu, X. Yang and S. Dang, *Appl. Catal., B*, 2011, **102**, 19–26.